A Brief Life and Death of a Torus: Computation of Quasiperiodic Solutions to the Kuramoto-Sivashinsky Equation

Adam M. Fox[a)]
Department of Mathematics, Western New England University, Springfield, MA 01119 USA

(Dated: 26 September 2015)

The Kuramoto-Sivashinsky equation (KSE) arises in the study of interfacial instability in a variety of settings such as flame-front propagation and the liquid film on an inclined plane. When only a single spatial dimension is considered the system can be parameterized by the length of the corresponding interval. As the spatial domain increases, the orbits of the Kuramoto-Sivashinsky system become increasingly turbulent. Quasiperiodic solutions are theorized to exist within this turbulence. These solutions lie on invariant tori which act as barriers to transport and are therefore of significant dynamical importance. We will present a numerical method to compute such orbits and describe their dynamics.

I. INTRODUCTION

Predicting the behavior of turbulent flows is exceptionally difficult. Analysis of the topologically invariant structures, as well as their stable and unstable manifolds, has proven fruitful in gaining insight into the dynamics of such systems.[1,2] The earliest studies focused on the simplest of such structures, namely the 0-dimensional equilibria. Later work extended these ideas to periodic orbits,[3,4] topologically 1-tori, and, to a lesser degree, quasi-periodic orbits,[5] which lie on higher dimensional tori.

In this paper we seek to further understand the role higher dimensional tori play in the dynamics of infinite dimensional chaotic dynamical systems. We study a quasi-periodic orbit that lies on a 2-torus in the Kuramoto-Sivashinsky system parameterized by the system size L. We show that such a 2-torus can come into existence when a nearby stable periodic orbit undergoes Hopf bifurcation and is later destroyed when it collides with an unstable periodic orbit. Unlike traditional KAM tori, this partially hyperbolic torus does not appear to be vulnerable to resonances.

In sect. II we introduce the Kuramoto-Sivashinsky equation and describe its utility in studying more general chaotic flows. We then present variational methods to compute periodic orbits and invariant tori in sect. III, first developed by Lan et al. We apply these methods to study the birth, life, and death of an invariant torus in sect. IV.

II. THE KURAMOTO-SIVASHINSKY EQUATION

The Kuramoto-Sivashinsky equation[6–8] is a simple yet physically intersesting nonlinear system that provides a foundation to study turbulence in more complex flows[8]. We will explore this system parametrized by the system size L,

$$u_t = (u^2)_x - u_{xx} - u_{xxxx}\,, \qquad x \in [0, L]\,. \tag{1}$$

Following Ref. 5 we will restrict our study to the antisymmetric solution space of (1) with periodic boundary conditions, i.e. $u(-x,t) = -u(x,t)$ and $u(x+L,t) = u(x,t)$, with $u(x,t)$ Fourier-expanded as

$$u(x,t) = \sum_{k=-\infty}^{\infty} i a_k e^{ikqx}, \tag{2}$$

where $q = 2\pi/L$ is the basic wavenumber and $a_{-k} = -a_k \in \mathbb{R}$. Accordingly, (1) becomes a set of ordinary differential equations :

$$\dot{a}_k = ((kq)^2 - (kq)^4)a_k - kq \sum_{m=-\infty}^{\infty} a_m a_{k-m}\,. \tag{3}$$

In the long-time limit of (3) for k large a_k's decay faster than exponentially, so a finite number of a_k's yields an accurate representation of the long-time dynamics. Previous studies[1,3–5] have shown that a truncation at $k = 16$ is sufficient for a quantitatively accurate calculation for the range of parameters that we are interested in.

III. NUMERICAL METHODS

III.1. Preliminaries

Here we describe a variational method to compute both periodic orbits[3] and invariant tori[5] in flows and maps of arbitrary dimension. Our presentation of these methods will be brief and we refer the reader to the original articles for a more detailed discussion. Since our primary goal is to examine the behavior of the Kuramoto-Sivashinsky equation we will restrict our presentation of this method to the continuous time case. We refer to reader to the original articles for details on the application of this technique to maps.

[a)] Electronic mail: adam.fox@wne.edu.

Let $\mathcal{M} \subset \mathbb{R}^d$ and $x \in \mathcal{M}$. We seek to compute periodic orbits and invariant tori of flows defined by first order ordinary differential equations

$$\frac{dx}{dt} = v(x). \tag{4}$$

For simplicity, we assume that the vector field $v(x)$ is sufficiently smooth.

The variational technique has the same basic approach for computing tori and periodic orbits. We begin with some initial guess $x(s,\tau)$ where s is a cyclic variable that parameterizes a loop. The variable τ acts as a "fictitious time" and parametrizes a continuous family of guess loops, with the initial guess at $\tau = 0$ and the true, desired orbit at $\tau = \infty$. In the following sections we derive the evolution rule of the loop under τ for the two cases.

III.2. Computation of Periodic Orbits

Let f be the flow of (4), that is $\frac{d}{dt} f^t(x) = v(x)$. A periodic orbit is determined by a pair (x, T), with $x \in \mathcal{M}$ and $T \in \mathbb{R}$, such that

$$f^T(x) = x.$$

We parameterize an initial guess for such an orbit $\tilde{x}_n = \tilde{x}(s_n, 0)$, with $\{s_0, s_1, \cdots, s_N\} \in [0, 2\pi]$, such that $\tilde{x}(s,0) = \tilde{x}(s+2\pi, 0)$. For simplicity we choose an evenly spaced grid, $\Delta s = 2\pi/N$. We define the s-velocity $\tilde{v}$ as the derivative of this loop with respect to s,

$$\frac{d\tilde{x}}{ds} = \tilde{v}(\tilde{x}). \tag{5}$$

The fundamental idea of this algorithm is that for any periodic loop the flow velocity must equal the s-velocity up to some constant, i.e. $\tilde{v}(\tilde{x}) = \lambda v(\tilde{x})$. The local time scaling factor

$$\lambda = \Delta t / \Delta s, \tag{6}$$

where $\Delta t = T/N$, serves to match the magnitudes of these tangents.

We must now construct a rule such that our initial guess loop $\tilde{x}(s,0)$ approaches a periodic orbit as $\tau \to \infty$. Let $x(t) = f^t(x)$ be the state of the system at time t and $J(x,t) = dx(t)/dx(0)$ be the corresponding Jacobian matrix. We compute this matrix by simultaneously integrating the system (4) and

$$\frac{dJ}{dt} = AJ, \; A_{ij} = \frac{\partial v_i}{\partial x_j}, \quad \text{where } J(x,0) = Id \tag{7}$$

We assume our initial guess is close to a true periodic orbit, $x_n = \tilde{x}_n + \delta\tilde{x}_n$, so that

$$f^{\Delta t + \delta t_n}(\tilde{x}_n + \delta\tilde{x}_n) = \tilde{x}_{n+1} + \delta\tilde{x}_{n+1}$$

Linearizing about $\tilde{x}_n$ and Δt yields

$$f^{\delta t}(x) \approx x + v(x)\delta t, \; f^t(x + \delta x) \approx x(t) + J(x,t)\delta x.$$

We can use these linearizations to construct the multiple-shooting Newton-Raphson equation

$$\delta\tilde{x}_{n+1} - J(\tilde{x}_n, \Delta t)\delta\tilde{x}_n - v(\tilde{x}_n)\delta t_n = f^{\Delta t}(\tilde{x}_n) - \tilde{x}_{n+1}. \tag{8}$$

Lan et al[3] showed that this Newton-Raphson iteration generates a sequence of loops with a decreasing cost function provided the initial guess is sufficiently close to the true periodic orbit.

We now iterate the system by $\delta\tau$, or, equivalently, multiply the right hand side of (8) by $\delta\tau$. We can simplify the result by noting

$$\delta t_n = \frac{\partial \lambda}{\partial \tau}(s_n, \tau)\delta\tau\Delta s \;\; \text{from (6) and} \tag{9}$$

$$\delta\tilde{x}_n = \frac{\partial}{\partial \tau}\tilde{x}(s_n, \tau)\delta\tau. \tag{10}$$

Dividing both sides of (8) by $\delta\tau$ thereby yields

$$\frac{d\tilde{x}_{n+1}}{d\tau} - J(\tilde{x}_n, \Delta t)\frac{d\tilde{x}_n}{d\tau} - v_{n+1}\frac{\partial\lambda}{\partial\tau}(s_n,\tau)\Delta s = f^{\Delta t}(\tilde{x}_n) - \tilde{x}_{n+1}. \tag{11}$$

Now, in the limit as $N \to \infty$ both Δs and Δt approach zero. This gives the estimates

$$v_{n+1} \approx v_n, \qquad f^{\Delta t}(\tilde{x}_n) \approx \tilde{x}_n + v_n\Delta t.$$
$$\tilde{x}_{n+1} \approx \tilde{x}_n + \tilde{v}_n\Delta s, \qquad J(\tilde{x}_n, \Delta t) \approx 1 + A(\tilde{x}_n)\Delta t$$

These approximations along with (6) yield the result

$$\frac{\partial^2\tilde{x}}{\partial s\partial\tau} - \lambda A\frac{\partial\tilde{x}}{\partial\tau} - v\frac{\partial\lambda}{\partial\tau} = \lambda v - \tilde{v} \tag{12}$$

This evolution equation describes the deformation of the initial guess loop $\tilde{x}$ to the true periodic orbit x.

For the discretized loop $\tilde{x}_n$ we approximate the s-derivative using a standard four-point approximation, $\tilde{v}_n = \frac{\partial\tilde{x}}{\partial s} \approx (D\tilde{x})_n$, where D is a block-diagonal matrix, see Ref. 3 for details. The evolution equation (12) of the discretized system is then

$$\begin{pmatrix} \hat{A} & \hat{v} \\ \hat{r} & 0 \end{pmatrix}\begin{pmatrix} \delta\hat{x} \\ \delta\lambda \end{pmatrix} = \delta\tau\begin{pmatrix} \lambda\hat{v} - \hat{\tilde{v}} \\ 0 \end{pmatrix}, \tag{13}$$

where $\hat{A} = D - \lambda\text{diag}[A_1, A_2, \cdots, A_N]$, $A_n = A(\tilde{x}(s_n))$, and

$$\hat{v} = (v_1, v_2, \cdots, v_N), \; v_n = v(\tilde{x}(s_n)), \tag{14}$$
$$\hat{\tilde{v}} = (\tilde{v}_1, \tilde{v}_2, \cdots, \tilde{v}_N), \; \tilde{v}_n = \tilde{v}(\tilde{x}(s_n))$$

are the vector fields whose direction we wish to coincide. The parameter $\delta\tau$ is the Euler step size used to solve the fictitious-time differential equation.

The Nd dimensional vector $\hat{r}$ imposes a constraint on the coordinate variations $\delta\hat{x} = (\delta\tilde{x}_1, \delta\tilde{x}_2, \cdots, \delta\tilde{x}_N)$. Note that every periodic orbit remains a periodic orbit under a cyclic permutation of its discretized points. The operation

$$\overline{A} = \frac{\partial}{\partial s} - \lambda A$$

used in (12) therefore has a marginal eigenvector $v(\tilde{x}(s))$ with zero eigenvalue. As we discuss below, the parameter λ is fixed in our implementation. Therefore, as $\tau \to \infty$,

$$\overline{A}\frac{\partial x}{\partial \tau} = 0$$

so $\overline{A}$ becomes singular and numerical issues arise. We remedy this problem by fixing the first coordinate of the first point of the discretized orbit $\tilde{x}_1(s_1, \tau) = const.$ The vector $\hat{r}$ ensures this point is fixed.

III.3. Implementation of the Algorithm

The first step in implementing this algorithm is choosing an appropriate guess loop. There are a variety of effective shooting methods that can be employed when attempting to compute an unstable or nonattracting stable periodic orbit, see Ref. 4 for examples. When computing attracting periodic orbits, such as those shown below, one can simply iterate a random orbit until it becomes sufficiently close to the attracting orbit and then use the result as the initial guess. This is the approach we used.

We employed a 256-point discretization for the loop $\tilde{a}_n$ (note that we now use a rather than x for the system (3)). The first point of this discretization was chosen on the Poincaré section $a_1 = 0.06$ and this point was evolved using (3) until the orbit returned to the $a_1 = 0.06$ section at time T_f. We then selected 256 points evenly spaced on the orbit so $\Delta t = T_f/256$ and $\Delta s = 2\pi/256$. The loop was then evolved using (13) and $\delta\tau = 1$ until the error $||\lambda v - \tilde{v}||_2 \leq 10^{-12}$. It is important to note that the error in this calculation is not the same at the error in the periodic orbit, ie $||f^T(a) - a||_2$.

An initial condition for the periodic orbit shown in Fig. 1 was generated by evolving a randomly selected point in the neighborhood as described above. The initial error $||\lambda v - \tilde{v}||_2 \approx 8.63 \times 10^{-4}$. This error dropped to 5.62×10^{-11} after one iteration and 2.73×10^{-14} after a second. The final error in the periodic orbit $||f^T(a) - a||_2 = 9.94 \times 10^{-7}$. This error could be reduced by increasing the number of points used in the discretization. The algorithm required approximately 20 seconds running on Matlab on a MacBook Pro laptop.

When the algorithm converged successfully at fixed L we used the result as the initial guess for the periodic orbits at nearby values of L. A more sophisticated extrapolation scheme may be more effective however we found the algorithm to be robust enough that it wasn't necessary.

III.3.1. Stability of Periodic Orbits in the Kuramoto-Sivashinsky System

Our discretization of the Kuramoto-Sivashinsky equation is 16-dimensional, so the linear stability of an orbit

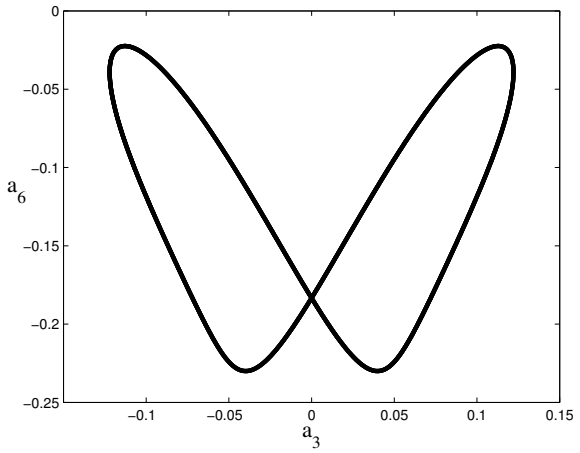

FIG. 1. A projection of a periodic orbit of the Kuramoto-Sivashinsky equation for $L = 41.2$. The return time is $T \approx 24.11$.

is described by the 16 eigenvalues Λ_j of its Jacobian matrix (7). If the orbit is periodic, the Floquet multiplier corresponding to perturbations along the orbit is unity. The observed periodic orbits of the Kuramoto-Sivashinsky equation have a few relatively large leading multipliers but the majority are strongly contracting, $|\Lambda_j| < 10^{-2}$ or less. These strongly contracting multipliers play a relatively insignificant role in guiding the overall dynamics. We will be primarily concerned with those few directions for which the magnitude of Floquet multipliers is relatively large, i.e. $|\Lambda_j| > 10^{-2}$.

III.4. Computation of Invariant Tori

Lan[5] demonstrated the existence of an invariant two-torus in the Kuramoto-Sivashinsky equation . To compute this torus we employ the *Poincaré section* method. In this method, one records the coordinates $\hat{x}_n$ of the trajectory $x(t)$ at the instants t_n when it traverses a fixed oriented hypersurface $\mathcal{P}$ of codimension 1. For the high-dimensional Kuramoto-Sivashinsky flow, the practical choice is a hyperplane.

The application of the Poincaré section method transforms the problem from computing a 2-torus in a continuous system to the computation of a 1-torus in a discrete one. A 1-dimensional torus is a closed loop on $\mathcal{P}$ which is invariant under the Poincaré map. We parameterize this loop $x(s)$ with $s \in [0, 2\pi)$ such that $x(s) = x(s+2\pi)$. The dynamics on the tori that we will examine are conjugate to a rigid rotation, that is

$$g(x(s)) = x(s + \omega)\,, \tag{15}$$

where g is the Poincaré return map and $\omega \in \mathbb{R}$ is the *rotation number*.

The initial guess loop $x(s, 0)$ is discretized by N points of dimension k that lie on $\mathcal{P}$. We construct a system of

ODEs in τ such that the error

$$F(s,\tau) = g(x(s,\tau)) - x(s+\omega(\tau),\tau)$$

goes to zero as $\tau \to \infty$. Note here that the shift ω may also evolve with τ. There are many choices one may make in this construction. We make the simple choice,

$$\frac{dF}{d\tau} = -F$$

yielding the differential equations

$$\frac{\partial x}{\partial \tau}(s+\omega(\tau),\tau) + \frac{\partial x}{\partial s}(s+\omega(\tau),\tau)\frac{\partial \omega}{\partial \tau}(\tau) - \tilde{J}(x(s,\tau))\frac{\partial x}{\partial \tau}(s,\tau) = F(x(s,\tau))$$

where $\tilde{J}$ is the Jacobian matrix of the Poincaré map g. This Jacobian is different than J, the Jacobian of the full system, however we can easily find $\tilde{J}$ from J.[9] Let $x' = g(x)$ be the first return to $\mathcal{P}$ of $x \in \mathcal{P}$, $v' = v(x')$, U be a function such that $U(x) = 0$ whenever $x \in \mathcal{P}$, and $U' = U(x')$. The Jacobian $\tilde{J}$ is then given by

$$\tilde{J}_{ij} = (\delta_{ik} - \frac{v_i' \partial_k U'}{v' \cdot \partial U'})J_{kj}.$$

If we are searching for an invariant 1-torus of a given topology, the shift $\omega = \omega(\tau)$ varies with the fictitious time τ, and is to be determined simultaneously with the 1-torus itself. Lan *et al.*[5] impose the *phase condition*[10]

$$\oint ds \left(v(s,\tau) \cdot \frac{\partial x}{\partial \tau}(s,\tau) \right) = 0\,, \tag{16}$$

which ensures that during the fictitious time evolution the average motion of the points along the loop equals zero. Empirically, for this global loop constraint the fictitious time dynamics is more stable than for a single-point constraint such as $\delta x(0,\tau) = 0$. For m-torus, $v(s,\tau)$ is a $[d \times m]$ tensor and (16) yields m constraints.

In practice, we expand x, $f(x)$, and the Jacobian matrix $\tilde{J}$ in terms of their Fourier series,

$$\begin{aligned} x(s,\tau) &= \sum_k a_k(\tau) e^{iks} \\ g(x(s,\tau)) &= \sum_k b_k(\tau) e^{iks} \\ \tilde{J}(x(s,\tau)) &= \sum_k \tilde{J}_k(\tau) e^{iks} \end{aligned} \tag{17}$$

Using this representation the artificial-time ODEs become

$$\left(\frac{da_k}{d\tau} + ika_k \frac{d\omega}{d\tau} \right) e^{ik\omega} - \sum_j \tilde{J}_{k-j} \frac{da_j}{d\tau} = b_k - a_k e^{ik\omega} \tag{18}$$

and the phase condition (16) is given by

$$\sum_k k a_k^* \frac{da_k}{d\tau} = 0 \tag{19}$$

and is solved simultaneously with (18). Solving this $[(dN+1) \times (dN+1)]$ system is the most numerically intensive component of the algorithm. We employ the LU factorization technique.

III.5. Implementation of the Algorithm

We first computed a torus at $L = 41.10$ using an $N = 16$ point discretization on the Poincaré section $a_1 = 0.06$ with an error threshold of 10^{-7}. An initial guess was generated by iterating a randomly chosen nearby point until it intersected Poincaré section N times, ignoring the first few transient intersections that occur before the orbit has settled onto the attracting torus. An initial estimate for the rotation number ω can be generated by minimizing the distance between the first return x' of a point x and the shift $x(s+\omega)$. This processes yielded an approximation of $\omega \approx 0.12$.

The system of $dN+1$ ODEs given by (18) and (19) is solved using the simple forward Euler method with step size 1. The initial error $||F(s,\tau)||_2 = 0.0016$ which fell to $||F(s,\tau)||_2 = 2.28 \times 10^{-8}$ after 6 iterations using $\delta\tau = 1$ and requiring 82 seconds running on Matlab on a Macbook Pro. This torus served as an initial guess for the torus at $L = 41.11$. In this case only 3 iterations and 47 seconds were required for convergence. Linear extrapolation was used to generate an initial guess for the torus at $L = 41.12$. Only two iterations and 36 seconds were required for convergence.

Additional care is needed when computing the torus for smaller values of L. As L becomes smaller the torus grows and becomes less circular, see Fig. 2. A larger discretization therefore becomes necessary to achieve the desired accuracy. Whenever the algorithm failed to converge to the desired accuracy the number of points in the discretization was doubled. This first occurred at $L = 41.06$ when N doubled to 32, and again at $L = 40.90$.

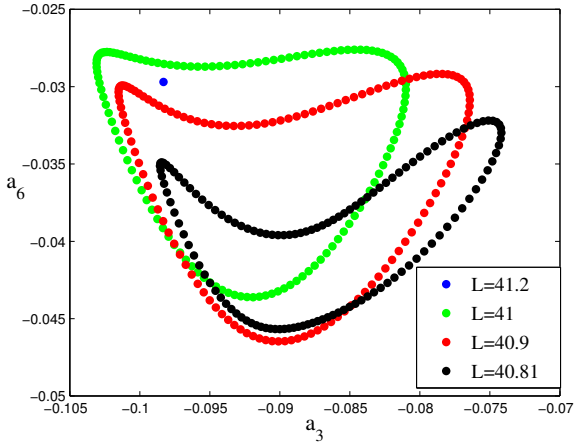

FIG. 2. Projection of the invariant tori of the Kuramoto-Sivashinsky equation over a range of parameter values.

IV. THE LIFE CYCLE OF AN INVARIANT TORUS OF THE KURAMOTO-SIVASHINSKY FLOW

When $L > 42$ we do not observe any invariant tori, however periodic orbits are abundant. One such periodic orbit, the one shown in Fig. 1, has three leading multipliers other than the unity multiplier: a single positive real multiplier less than one, and a complex pair $\{\Lambda_j, \Lambda_{j+1}\} = \{\exp(\theta_j)|\Lambda_j|, \exp(-\theta_j)|\Lambda_j|\}$ with moduli less then unity. As L decreases the moduli of these multipliers increase and, at $L \approx 41.95$, becomes one. The resulting Hopf bifurcation gives birth to an attractive two-torus, shown in Fig. 2, analogous to the limit cycles seen in bifurcations of equilibria.

As L continues to decrease two significant phenomena occur. First, the invariant torus grows larger, as can be seen in Fig. 2. Secondly, the periodic orbit contained within the torus undergoes an additional bifurcation, see Fig. 3. At $L \approx 40.84$ the complex eigenvalues of the periodic orbit collide causing the orbit to become unstable. A new stable periodic orbit is also generated, see Fig. 3.

Although the torus does grow as L decreases it is still quite narrow even at its largest. Indeed, the quasi-periodic orbit on the torus and the periodic orbit in the interior of the torus are visually indistinguishable. It is therefore unclear how dynamically important this particular torus is.

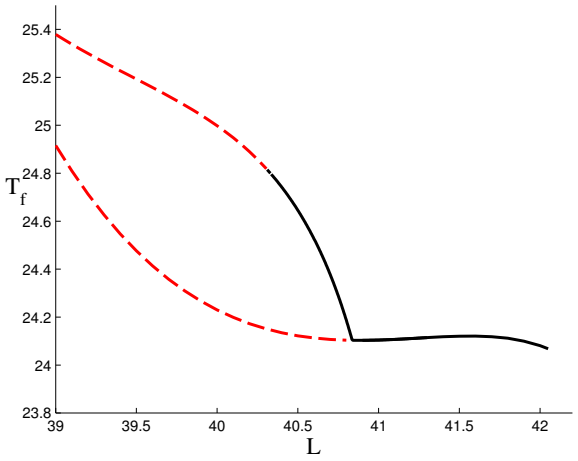

FIG. 3. Bifurcations diagram of the periodic orbits nearby the invariant torus. The dashed red line indicates an unstable orbit while the solid black line indicates a stable orbit.

Previous studies of symplectic and volume-preserving systems have shown that the growth of a Sobolev seminorm can be used to predict the breakdown of tori[11–13]. We define this seminorm as

$$||\overline{a}_k||_m^2 = \sum_j (2\pi|j|)^{2m} |\overline{a}_k|^2 \,, \tag{20}$$

where $\overline{a}_k$ are the Fourier coefficients of the k^{th} dimension of a. A plot of $||\overline{a}_2||_3^2$ for L near the destruction of the torus is shown in Fig. 4. The value of the seminorm appears to become infinite at a some critical value, L_{cr}. At L_{cr} the torus loses analyticity and, we assert, ceases to exist. We can estimate L_{cr} by modeling the data as a pole,

$$||\overline{a}_k||_m^2 \sim \frac{\alpha}{(L - L_{cr})^\beta} \,. \tag{21}$$

A nonlinear least squares fit using the final 5 points gives $L_{cr} \approx 40.8027 \pm 4 \times 10^{-4}$. This value was consistent for different values of m and k and number of points used.

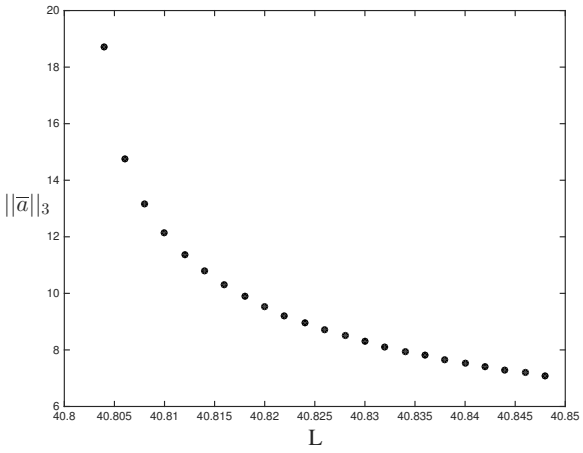

FIG. 4. Values of the Sobolev seminorm (20) with $m = 3$ of the Fourier coefficients of a_2. This norm becomes infinite at $L_{cr} \approx 40.8027 \pm 4 \times 10^{-4}$.

The destruction of the torus appears to be caused by a collision between the torus and the periodic orbit shown in Fig. 1, which is unstable for $L < 40.84$, recall Fig. 3. To test this hypothesis we computed the minimum distance between the periodic orbit and the torus over a range L values, see Fig. 5. Specifically, we examined the distance on the (a_3, a_6) projection on different Poincaré sections $a_1 = const$ and found the minimum distance over all sections. The 5 points closest to the collision were fitted to a pole, as in (21), yielding an estimate of the collision parameter of $L_{cr} = 40.8019 \pm 7 \times 10^{-4}$. The close agreement of this estimate to the one derived from the Sobolev norm provides strong numerical evidence of the validity of both techniques.

IV.1. Rotation Numbers of the Invariant Tori

The rotation number ω of the torus is fixed by the dynamics and determined by the phase condition (19). Unlike KAM tori, whose rotation numbers must be sufficiently irrational[14], this partially hyperbolic torus does not exhibit any sensitivity to resonance, as shown in Fig. 6. Indeed, we examined the region near $\omega = \frac{1}{10}$ more closely and found no evidence that the torus was affected by the resonance.

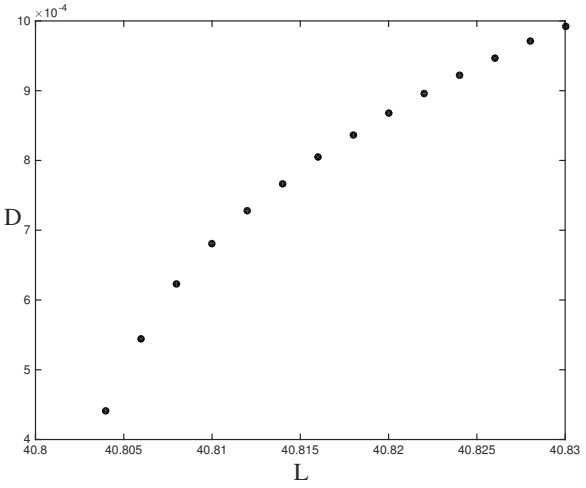

FIG. 5. Minimum distance between the unstable periodic orbit shown in Fig. 1 and the torus surrounding it. The periodic orbit collides with the torus at $L_{cr} = 40.8019 \pm 7 \times 10^{-4}$

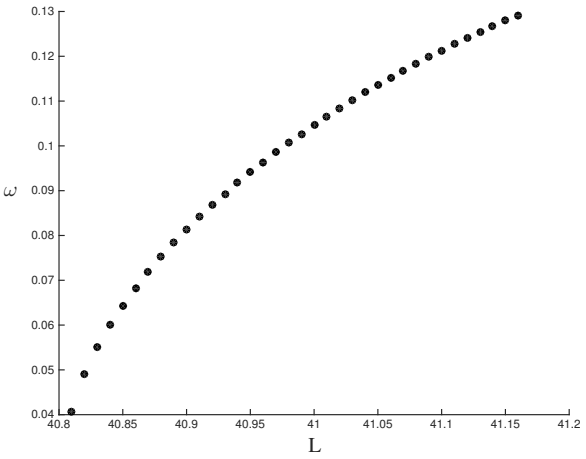

FIG. 6. Rotation number ω of the invariant tori of the Kuramoto-Sivashinsky equation for different system sizes L. The torus does not appear vulnerable to resonances.

V. CONCLUSIONS

In this paper we explored the life cycle of an invariant torus of the Kuramoto-Sivashinsky system. We showed that the birth and death of a such a torus can be determined by studying the periodic orbit contained within the interior of the torus. We also demonstrated that the torus is robust to resonance in the rotation number of the orbit.

As we had noted in sect. IV, the torus we compute is narrow and is therefore presumably of little importance for the computation of dynamical averages. There may be other tori in the Kuramoto-Sivashinsky system that are larger, occupying a significant region in phase space. These tori could have a remarkable role in the dynamics, and appreciably advance our understanding of these systems. The results and methods described in this paper will allow us to begin searching for such consequential invariants.

ACKNOWLEDGMENTS

The life & death question was posed by P. Cvitanović, whose advice was helpful throughout this project. Author is also indebted to Y. Lan and J.D. Meiss for inspiring discussions. Author acknowledges support by NSF grant DMS-1162544 and Western New England University.

[1] F. Christiansen, P. Cvitanović, and V. Putkaradze, "Spatio-temporal chaos in terms of unstable recurrent patterns," Nonlinearity **10**, 55–70 (1997).

[2] B. Hof, C. W. H. van Doorne, J. Westerweel, F. T. M. Nieuwstadt, H. Faisst, B. Eckhardt, H. Wedin, R. R. Kerswell, and F. Waleffe, "Experimental observation of nonlinear traveling waves in turbulent pipe flow," Science **305**, 1594–1598 (2004).

[3] Y. Lan and P. Cvitanović, "Variational method for finding periodic orbits in a general flow," Phys. Rev. E **69**, 016217 (2004), arXiv:nlin.CD/0308008.

[4] P. Cvitanović, R. L. Davidchack, and E. Siminos, "On the state space geometry of the Kuramoto-Sivashinsky flow in a periodic domain," SIAM J. Appl. Dyn. Syst. **9**, 1–33 (2010), arXiv:0709.2944.

[5] Y. Lan, C. Chandre, and P. Cvitanović, "Variational method for locating invariant tori," Phys. Rev. E **74**, 046206 (2006), arXiv:nlin.CD/0508026.

[6] Y. Kuramoto and T. Tsuzuki, "Persistent propagation of concentration waves in dissipative media far from thermal equilibrium," Progr. Theor. Phys. **55**, 365 (1976).

[7] G. I. Sivashinsky, "Nonlinear analysis of hydrodynamical instability in laminar flames - I. Derivation of basic equations," Acta Astr. **4**, 1177 (1977).

[8] P. Holmes, J. L. Lumley, G. Berkooz, and C. W. Rowley, *Turbulence, Coherent Structures, Dynamical Systems and Symmetry*, 2nd ed. (Cambridge Univ. Press, Cambridge, 2012).

[9] P. Cvitanović, R. Artuso, R. Mainieri, G. Tanner, and G. Vattay, *Chaos: Classical and Quantum* (Niels Bohr Institute, Copenhagen, 2014) ChaosBook.org.

[10] F. Schilder, W. Vogt, S. Schreiber, and H. M. Osinga, "Fourier methods for quasi-periodic oscillations," Int. J. Numer. Meth. Engng **67**, 629–671 (2006).

[11] R. Calleja and R. de la Llave, "Computation of the breakdown of analyticity in statistical mechanics models: numerical results and a renormalization group explanation," J. Stat. Phys. **141**, 940–951 (2010).

[12] R. Calleja and R. de la Llave, "A numerically accessible criterion for the breakdown of quasi-periodic solutions and its rigorous justificaition," Nonlinearity **23**, 2029–2058 (2010).

[13] A. M. Fox and J. D. Meiss, "Critical invariant circles in asymmetric and multiharmonic generalized standard maps," Comm. Nonlinear Sci. Numer. Simulat. **19**, 1004–1026 (2014).

[14] R. De La Llave, "A tutorial on KAM theory," in *Smooth ergodic theory and its applications (Seattle, WA, 1999)*, Proc. Sympos. Pure Math., Vol. 69 (Amer. Math. Soc., Providence, 2001) pp. 175–292.